The third KV62 radar scan: Searching for hidden chambers adjacent to Tutankhamun's tomb

ACCEPTED FOR PUBBLICATION IN ***JOURNAL OF CULTURAL HERITAGE***

The third KV62 radar scan: Searching for hidden chambers adjacent to Tutankhamun's tomb.

[1]L. Sambuelli[1], C. Comina[2], G. Catanzariti[3], F. Barsuglia[4], G. Morelli[4] and F. Porcelli[5].

[1]Department of Environment, Land and Infrastructures, Polytechnic University of Turin, Italy.

[2]Department of Earth Sciences, University of Turin, Italy.

[3]3DGeoimaging, Torino, Italy.

[4]Geostudi Astier s.r.l., Livorno, Italy.

[5]Department of Applied Science and Technology, Polytechnic University of Turin, Italy.

Abstract

The existence of hidden chambers and corridors adjacent to Tutankhamun's tomb (code name KV62) has been long debated. In 2015 it was suggested that these chambers may host the as yet undiscovered burial of Nefertiti. In order to test this hypothesis, two Ground Penetrating Radar (GPR) surveys, conducted in 2015 and 2016 from inside KV62, were carried out, but gave contradictory results. To solve these uncertainties and obtain a more confident and conclusive response, a third GPR survey was conducted by our team in February 2018. The results of this third radar scan are reported in this article. Three GPR systems with multiple frequency bands (from 150 MHz to 3000 MHz) and very dense spatial sampling were adopted. After careful data processing, no evidence of marked discontinuities due to the passage from natural rock to artificial blocking walls were found in the radargrams. It is therefore concluded that there are no hidden chambers immediately adjacent to the Tomb of Tutankhamun.

Keywords: Valley of the Kings; KV62 tomb; Tutankhamun; GPR.

1. Introduction and research aim

The tomb of the young pharaoh Tutankhamun is the most famous of all the royal tombs within the Valley of the Kings (VOK) in Luxor. This tomb was discovered, with an almost intact funerary treasure, by Howard Carter in 1922 (Carter and Mace, 1923) and it is referred to as KV62 in the standard Egyptological designation. The site of the burial is cut into the floor of the VOK within the natural bedrock, which belongs to the lower member of the Theban Limestone Formation (see, e.g., Aubry et al., 2009; Dupuis et al., 2011). The tomb was prepared in a limited time due to the sudden death of the young pharaoh and is much smaller than most royal tombs in the VOK.

In 2015, Egyptologist Nicholas Reeves proposed a theory (Reeves, 2015) according to which Tutankhamun's tomb may be part of a larger tomb belonging to Queen Nefertiti. Reeves' hypothesis was based on the examination of high-resolution 3D laser-scan photos taken by Factum Arte to create a digital replica of KV62 painted walls (Factum Arte, 2015). Reeves identified, beneath the plastered surfaces of the painted KV62 walls, distinct linear traces that he interpreted as the "ghosts" of two hitherto unrecognized doorways leading to hidden chambers and corridors (Reeves, 2015). These supposed doorways appear to be located across the right portions of the North and West walls of Tutankhamun's funerary chamber (see later Fig. 2). Reeves speculated that these doorways were sealed with stones and later covered with plaster in preparation of Tutankhamun's funerary chamber. Presumably, the sealing of these doorways should be similar to the one found by Carter at the entrance to KV62, constituted by a blocking masonry wall made of blocks and of rough slabs of varying size covered with smaller stones, forming the external layer of the filling, and an eventual wooden lintel situated on top (Carter and Mace, 1923).

In order to test Reeves hypothesis, the Egyptian Ministry of Antiquities (MoA) commissioned a first Ground Penetrating Radar (GPR) scan of Tutankhamun's tomb, carried out by a H. Watanabe in November 2015 (Watanabe, 2015). Indeed, GPR techniques are the most effective method to establish the presence of hidden chambers adjacent to KV62, given the expected physical contrast between the bedrock in which KV62 is carved and the supposed sealed doorways, together with the marked lateral discontinuity that should be present at the corners of these doors, as well as the possible presence of a wooden lintel above

the doors. GPR is commonly and successfully used in archeological and forensic applications (e.g. Daniels, 2004; Goodman and Piro, 2013). This first GPR survey employed a modified Koden KSD-3AM 400 MHz GPR to investigate specific parts of Tutankhamun's tomb. The results seemed to confirm Reeves' hypothesis. In particular, Watanabe's interpretation indicated the presence of two distinct regions (or cavities) of significant empty space beyond the decorated North and West walls of the burial chamber. Furthermore, based on further speculations he suggested also the presence within these cavities of metallic and organic substances (Watanabe, 2015).

This finding was called "the discovery of the century" and was reported by news and media around the world (see, e.g, El-Aref 2015; Michaelson and Walker, 2016). The MoA then commissioned a second GPR survey to reconfirm the results of the first KV62 GPR survey. This second survey was carried out by a National Geographic team in March 2016, using a SIR4000 GPR (GSSI) and two antennas, of 400 MHz (Model 50400S, GSSI) and 900MHz (Model 3101, GSSI), to scan into the walls of the tomb. The antennas were mounted horizontally and installed on a camera 'slider' rail system, which allowed over forty scans to be taken horizontally across the wall at multiple vertical positions (National Geographic Society, 2016). The survey was also supposed to provide crucial information for the planned operation of a specially constructed drill capable of drilling a small hole through which a probe could be inserted into the presumed cavities (Hiebert, 2016). However, the second KV62 GPR scan could not confirm the initial findings by Watanabe. In their report , the National Geographic team concluded that no large voids were detected, and no proposed chamber walls could be observed. Therefore, the conclusions of the second KV62 GPR survey were inconsistent with those of the first GPR survey (National Geographic Society, 2016).

Given this state of affairs, the MoA called for a third, comprehensive geophysical survey of the tomb of Tutankhamun capable of providing conclusive evidence on the question of the existence of hidden chambers and corridors adjacent to KV62. Our team was invited to submit a project proposal, entitled "The third KV62 radar scan: Advanced Technologies applied to the search for void areas and underground structures adjacent to the Tomb of Tutankhamun", which was later approved by the Permanent Committee

of the MoA. This article focuses on the results of this project and of the related GPR surveys conducted in February 2018.

The fact that the two previous KV62 radar scans proved inconclusive was a strong indication that the complexity of the task was somehow underestimated. Therefore, in order to counter potential technical difficulties, we decided to carry out the third survey utilizing three GPR systems covering multiple frequency bands, from 150 MHz to 3 GHz. High frequency surveys allow higher resolution for a potential identification of shallow anomalies related to the doorways corners and to the presence of a backfilling structure made by incoherent material, including non-shaped stones blocks. Low frequency GPR surveys promote electro-magnetic (e.m) wave penetration and the potential identification of deeper voids. In addition, different (i.e., vertical and horizontal) antenna polarizations were adopted. An *ad hoc* frame for the horizontal scanning of the high frequency GPR and an *ad hoc* lifter for vertical scans of the low and intermediate frequency GPR were designed and realized by our team. A significantly denser survey spacing than in the two previous investigations was planned in order to cover the interested walls with greater accuracy and to carry out a full 3D GPR survey. We decided to carry out GPR scans in the course of a seven-day period, with two four-hour sessions per day. This strategic planning allowed us to confront unforeseen complexities, which arose in the first two days of the surveys, and to come up with technical solutions. We considered important not only to acquire enough high-quality data, that would allow reaching a conclusive answer on the possible existence of hidden chambers adjacent to KV62, but also to provide a plausible explanation of why the previous two radar scans gave contradictory results. At the end, the collected data obtained in the course of a very large number of horizontal and vertical scans of the relevant KV62 walls summed up to about 2.7 km of radagrams, which is estimated to be about one order of magnitude more than those collected by the two previous KV62 GPR surveys combined. This paper discusses how we measured, processed and interpreted this huge amount of data. It is worth mentioning that a fourth, low-frequency unshielded high-power GPR antenna, capable of penetrating several meters, was also provided by Terravision, a geophysical company based in the UK, within the framework of our project. The Terravision team joined us in Luxor and carried out measurements within the tomb during two sessions.

The Terravision team was also supposed to work outdoor looking down underground from the top of KV62 but they could not complete such planned data acquisition.

Our investigation could also benefit from data and information of an Electrical Resistivity Tomography (ERT) survey in the area surrounding Tutankhamun's tomb performed by our team in May 2017 (Fischanger et al., 2018, and Porcelli et al., 2018). The ERT imaging showed two anomalies located underground a few meters from Tutankhamun's tomb, although no evidence of a corridor or empty spaces adjoining these anomalies with KV62 was found in the ERT data. Therefore, in addition to testing Reeves' hypothesis and understanding the results of the two previous radar scans, the third KV62 radar survey was also intended to establish whether a passageway of some sort existed connecting Tutankhamun's tomb to the two newly found ERT anomalies.

2. Material and methods

We adopted three different frequency bands (Low Frequency (LF) 150-200 MHz, Intermediate Frequency (IF) 600-900 MHz and High Frequency (HF) 1500-3000 MHz) for the surveys, with scans along vertical and horizontal directions and very close profile spacing (see Supplementary Material) in order to obtain a very dense spatial sampling. We moreover employed double antenna polarizations, with transmitting and receiving dipoles both orthogonal (TE - Transverse Electric mode) and parallel (TM - Transverse Magnetic mode) to the profile direction. Due to the requirement of scanning the walls without damaging their precious decorations, a special equipment was designed and realized by our team in order to move the antennas at a certain distance from the walls. As a consequence of the significant irregularities of the KV62 burial chamber walls, we therefore acquired the data at variable distances from the wall surface, roughly ranging between 0.05 and 0.1 m.

A common reference system was used for a mutual positioning of the different surveys. This reference system has its origin in the SW corner of the KV62 burial chamber (see Fig. 1), with the x-axis parallel to the North wall, the y-axis parallel to the West wall and the z-axis representing the height from the floor. We aslo collected calibration sections, for all three frequency bands used, in different positions within the burial

chamber and the surrounding rooms in order to evaluate the ability of the adopted radar systems to recognize known voids or back-wall structures. The location of the calibration profiles is depicted in Fig. 1. In the following, the acquisitions performed with the different radar systems are briefly discussed, further details on the acquisition and profile distribution are provided in the Supplementary Material section.

2.1 High Frequency (HF) scans.

We planned the HF scans in order to investigate a stripe, about 1.5 m high, along the West and the North walls. We realized the stripe in segments, or panels, each one about 1.5 m long, by means of an on-purpose built wooden frame resting on a flat platform (see Supplementary Material). We moved both the frame and the platform after the complete scanning of a single panel was achieved. Each panel is composed of several horizontal scans, obtained by sliding the antenna on a horizontal wooden bar starting from the bottom of the panel (located at approximately 0.75 m from the floor) to its top. Figure 2 represents a sketch of the frame positions and of the area covered by HF scans along the West and North walls. As it can be observed, panels are partly overlapping and a superposition of the frame positions has been adopted in some locations. In Figure 2 c and d numbering refers to traces identified by Reeves on the 3D laser-scan photos and to his speculation on these traces.

We acquired all the GPR profiles with a GPR unit composed by an Aladdin 2GHz IDS antenna box and an IDS K2 control unit. A wheel encoder was used to track the position of the antenna along the sliding bar for each GPR profile. The Aladdin box has two couples of transmitting and receiving dipoles: orthogonal (TE mode) and parallel (TM mode) to the profile direction. Signals from both these modes of operation can be transmitted and acquired simultaneously. We acquired data for a trace duration of 40 ns and 1024 samples per trace at a sampling frequency of 25.6 GHz. The trace interval in the scan direction was of 0.01 m while the scan spacing in the vertical direction (approximately depicted in Figure 2) was of 0.04 m. Each panel is on average composed of 78 radargrams (39 for each acquisition mode). The total number of acquired radargrams for the two modes along the North and the West walls of KV62 funerary chamber is therefore 546, for an acquisition length of about 820 m.

2.2 Low Frequency (LF) and Intermediate Frequency (IF) scans.

We acquired LF scans with an IDS RIS TR200 shielded antenna operating in TE mode. The antenna unit was driven by a DAD-MCH fast wave control unit and was vertically deployed along the burial chamber walls by means of an electrical aluminum lifter specifically designed and developed for the present surveys. In order to trigger the pulse emission and to record GPR traces at fixed space intervals, an optical encoder was mounted on the axis of a pulley winch connected to the lifter engine. We collected data along the vertical direction, from bottom to top (Figures 3a and 3b).

On average, we scanned the investigated walls at a height between 0.3 and 2.5 m from the floor. We acquired data for a trace duration of 128 ns and 1024 samples per trace at a sampling frequency of 8 GHz. We recorded traces each 0.003 m along the profile direction whilst spacing between adjacent profiles was set to 0.2 m. We acquired a total of 51 profiles, for an acquisition length of about 100 m.

We acquired IF scans with a dual polarization multi-channel IDS Stream-C system. The same aluminum lifter used for LF scans was adopted to slide up and down the multi-channel antenna along the walls (Figure 3c). The Stream-C allowed to simultaneously record, by a single swath, 23 radar profiles in TM-mode and 9 radar profiles in TE-mode. The Stream-C multi-antenna has indeed TM and TE arrays centered along two parallel horizontal axis vertically shifted by 0.19 m, with a channels spacing of 0.0435 (TM) and 0.099 m (TE), respectively. We acquired data for a trace duration of 80 ns and 512 samples per trace at a sampling frequency of 6.4 GHz. The trace interval in the scan direction was of 0.003 m. A total of 452 closely spaced dual polarized radar profiles were collected during IF scans, for an acquisition length of about 530 m.

3. Results

The three collaborating groups processed the data acquired with the different GPR systems independently and with different software, to avoid biasing and cross influences. Only after a satisfying processing step was reached we discussed and uniformed the processing flow in order to obtain a consistent result for all the surveys. Details on the processing flow adopted for the different radar systems are reported in the Supplementary Material section.

Successful imaging of known voids and structures (notably, the Annex and the Treasury in KV62) over calibration profiles was used to test the data processing flow and to evaluate the potentiality and limitations of the adopted surveying approach. Details of the results obtained over calibration profiles are reported in the Supplementary Material section. Here, the main results of the calibration procedure are summarized as follows:

- a reliable estimation of the propagation velocity (0.12 m/ns) of the GPR pulse in the rock around the tomb was obtained from diffraction hyperbolae;

- a clear void identification over known wall thickness ranging from 0.55 m (wall separating the Burial Chamber from the Treasury Chamber) to 0.8 m (wall between the Antechamber and the Annex) was observed; conversely, both IF and LF calibration profiles performed along the south wall of the Burial Chamber (for exact location see Figure 1) failed in locating the known void of the Annex at about 5 m depth. This indicated that attenuation factors were higher than expected; therefore, smaller maximum investigation depths, particularly for LF scans, should be expected.

3.*1 Wall scans.*

Figure 4 illustrates examples of the results obtained by the High Frequency (HF) scans. Sections taken from the 3D-assembled processed HF scans are shown in Figure 4a. The adopted reference system is the one shown in Figure 1. The color scale used for the representation of all the radargrams is based on the Normalized Absolute Amplitude of Reflection (NAAR) saturated at 0.25 to enhance lower values.

The results presented are typical examples of the ones obtained over the whole investigated volume. Higher reflection amplitudes are generally observed in the first 0.5 m, along the scanned walls. There are explanations for this phenomenon. First, we did not recover all the energy of the pulse as it propagates into the rock. In fact, the intrinsic attenuation of the material is not well known, therefore we simply applied a typical gain compensating for the spherical divergence of the signal. If, on one hand, the choice of a higher gain could magnify other deeper reflections, on the other hand it could enhance noise and/or ghost signals. Secondly up to a depth of 0.5 m into the wall, the signal could be affected by a higher fracture density because of the physics of pick excavation. These widespread fractures could result in the spread reflections visible in nearly all the radargrams within a depth of 0.5 m into the walls.

Along the North wall from x-coordinate values between 1.6 to 2.2 m (indicated by area 1 in Figure 4a), the reflection amplitude at shallow depth is enhanced due to the presence of a well-known wall repair (Wang et al., 2012b). We did not noticed other marked shallow anomalies along the walls even at different elevations. Near the top of the N-W section, at a depth of about 2 m, a linear reflection is also clearly visible (indicated by area 2 in Figure 4a). This is the only deep reflection that has been identified from HF scans within all the investigated volume. In Figure 4b, the orientation of this linear reflection is better visualized. At about two meters behind the North wall horizontal and vertical sections of the 3D volume evidence the traces of a plane sub-parallel to the North wall and dipping North of about 80° (dipping plane in Figure 4b). The presence of this reflection is important for two reasons: given its clear visibility, it is an indication that the investigation depth is likely around 2 m; furthermore, It is a clear evidence of a natural fracture belonging to a well-recognized sub-vertical EW fracture system (Dupuis et al., 2011). This means that the GPR pulse likely travels in the host rock only, since it does not intercept other reflecting surfaces due to anthropic structures between the wall and the aforesaid fracture.

Results obtained for LF and IF scans are similar to the ones reported for HF scans and are illustrated by Figure 5. Horizontal and vertical cross sections resulting from 3D-assembling and data processing are shown in this figure. Along the North wall, in a similar position than for HF scans, the increased reflection amplitude due to the wall repair can be noted both in the horizontal cross sections (A in Figure 5a and b)

and in the vertical ones (A in Figure 5d). In the horizontal cross sections this effect is, for both LF and IF scans, more localized and persistent with increasing time with respect to HF scans. The extension of the wall repair is however very clear and localized as shown in a vertical cut at 0.6 m depth from the IF GPR volume (A in Figure 5d). As previously discussed, the profiles acquired along the South wall failed in identifying the known void volume corresponding to the Annex (Figure 5a and b) while a clear evidence of the wall separating the Burial Chamber from the Treasury Chamber is observable for both Lf and IF scans (B in Figure 5a, b and c). Given these results, we can therefore assume that investigation depth from LF and IF scans are limited to about 3-4 m.

In IF scans, a deep linear reflection can be also noted behind the West wall (C in Figure 5b). This reflection can be caused by a fracture within the rock mass, similarly to the one reported for HF scans. An alternative explanation could be also a rebound effect of the radar pulse from the opposite east wall of the Burial chamber. No other relevant anomalies result from the scans also at different elevations within the 3D volume. This can be further observed in Figure 6, where representative IF radargrams, showing the response recorded from the KV62 burial chamber walls, are reported.

4. Discussion

We consider the results obtained from the processing and the interpretation of the third KV62 radar scan sound and definitive with a high degree of confidence. However, there are few open questions that deserve a discussion and may be the subject of further work.

In High Frequency (HF) profiles, the effect of the frame supports are stronger than in preliminary tests carried out on other masonry walls outside the tomb. Even though some diffraction hyperbolas were visible in these preliminary tests, they had an energy significantly lower than those recorded within KV62. These observations suggest that the electromagnetic properties (permittivity, permeability, conductivity) of the plaster supporting the paintings is very different from the ones of the natural rock, therefore strongly influencing wave propagation. Given the considerable humidity of the KV62 burial chamber, water could have penetrated the shallow surface, therefore lowering the resistivity of the plaster and transforming this

variable-thickness layer in a conductor. The superficial plaster layer could act as a wave-guide, inducing the e.m. waves traveling in the plaster to leak toward the room and be scattered back from the aluminum and wooden supports, giving rise to the diffraction hyperbolae observed in the radargrams. A similar effect could cause also the rebound reflections observed in Intermediate Frequency (IF) scans. In order to simulate the reliability of this scenario, appropriate values of the e.m. properties of both the plaster and the rock behind are needed. Indeed, it is known that the host rock belongs to the lower member of the Theban Limestone Formation, but it is not clear if it is a limestone, a marly limestone or a marl (see, e.g., Aubry et al., 2009; Dupuis et al., 2011). From our earlier ERT surveys carried out on the hill above KV62 (Fischanger et al 2018; Porcelli et al., 2018), we found that the rock surrounding the tomb had an average value of resistivity ρ (at zero frequency, i.e. under continuous current) of about 3000 Ohm-m. The propagation velocity of the GPR pulse obtained from our calibration tests inside KV62 is consistent with a value of relative permittivity ε of about 6.25 (see also National Geographic, 2016). Then, assuming a relative permeability μ equal to 1, a calculation using Maxwell and radar range equations (e.g. MIlsom and Eriksen, 2011) indicates that, with the 200 MHz antenna, a reflection of the North wall of the Annex, at 5 m distance from the South wall of the Burial Chamber, should be visible at about -45dB. Taking into account also the other losses due to the pulse impinging on the wall surface and to the system performance, a 90 dB system should be able to detect the reflected pulse. On the other hand, the rock resistivity may be a function of the e.m. wave frequency, and at the GPR frequencies adopted in our survey it may differ substantially from the one obtained with continuous current (as with ERT). If the resistivity of the limestone at 200 MHz were 500 Ohm m (Vaccaneo et al., 2004), the calculation with the same values of the other parameters would lead to a reflection at about -55 dB. Higher attenuations are clearly to be expected in the higher frequency range. We therefore believe that the missing reflected signal is due to either the air gap between the antennas and the wall, or to the intrinsic attenuation of rock and plaster, or a combination of these two effects. A laboratory estimate of the e.m. properties of the rock hosting KV62 would then be desirable. With guided wave devices (Vaccaneo et al., 2004), it should be possible to have, at least in laboratory on rock samples, a good estimate of the e.m. properties of a rock material within the GPR frequency band.

It is also still to be evaluated, particularly in HF band acquisitions, how much the variable dipole-wall distance and the different thickness of the plaster affect the signal. In order not to touch the paintings, the antennas mounted on the frames were moved on virtual planes nearly parallel to the walls. In fact, the walls inside KV62 are not smooth planes; rather, they present a waving surface that can differ from an ideal interpolating plane by 0.01 to 0.05 m. This means that even if the acquired profiles lay on a plane, there can be a variable thickness of air between the antenna and the wall. Especially in HF band, which has a dominant wavelength in air equal to 0.15 m, this air gap could play an important role both in the amount of energy entering the wall and in the banding noise (horizontal stripes) within the GPR records. Moreover, and very likely, the plaster has different thickness along the walls. This difference can affect pulse propagation and absorption.

5. Conclusions

According to the processed data from High Frequency (HF) acquisitions, we can state that all the radargrams appear to be substantially similar along the investigated walls: no marked lateral discontinuities due to the passage from natural rock to artificial blocking wall are evidenced. In other words, no evidence is found of a vertical plane (orthogonal to the scanned walls) that could be interpreted as the boundary between the rock and a blocking wall. Nor we see reflections attributable to the jambs or the lintel of a door. Within the depth investigated by HF scans (about 2 m), there is no evidence of plane reflectors (parallel to the scanned walls) that could be interpreted as chamber walls, like the ones seen in calibration profiles. Conversely, we see at least a clear fracture within the natural host rock in a particular location.

According to the data analysis and post-processing from Low and Intermediate Frequency acquisitions we can state that, within an estimated maximum investigation depth of 3-4 m, the radargrams show a homogenous response not supporting the presence of voids (i.e. empty chambers) or masonry structures concealing blocked doors. Both LF and IF datasets show apparent vertical discontinuities and ringing effects caused by the acquisition conditions and provide a different response on the sector of the Northern wall where an ancient wall repair exists. This response, probably emphasized by the air gap between the

antenna and the wall surface, gives a clear idea of the effects that can be caused on the GPR signal by a relative thin patch interrupting the dielectric continuity of the natural host rock. On this basis, and according to our experience, similar or stronger effects distributed over larger areas would have been expected if an artificial blocking made by splinter of limestone was present. However, this type of effects were not visible in the data.

Our work suggests that the first KV62 GPR survey was likely misled in its conclusions by *ghost signals*, i.e., rogue radar reflections originating in front of the walls, not beyond them. Under normal circumstances, a GPR antenna sends radar waves straight through the wall, and they bounce right back to the receiver, providing a very clear signal. But it appears that in KV62, only part of the radar waves went through, while the other part traveled along the walls surfaces before returning to the receiver. There are many suspected reasons for this complex behavior. First of all, for totally understandable reasons, we were not allowed to slide the antennas directly over the painted walls. Thus, the e.m. waves traveled first through an air layer of variable thickness between 0.05 and 0.1 m, as KV62 walls are not perfectly smooth and vertical. This fact, on one hand, limited the amount of e.m. wave energy going directly through the wall and, on the other hand, posed a challenge to the required level of accuracy in monitoring the relative position between the antennas and the walls. Secondly, beyond the air layer, the e.m. waves had to go through a plaster of variable thickness, whose e.m. properties are not exactly known. As a first approximation, the plaster could be thought of as made of powder from the local shale (huba), with the addition of some organic material. Despite the many tests on plaster samples taken from KV62 and other tombs (see, e.g., Wong et al., 2012a and 2012b; Wust and McLane, 2000), no dedicated tests on its e.m. properties, nor data on its actual water content, are available. In any event, due to combined presence of organic materials and moisture, the plaster appears to be able to conduct electricity and thus to play the undesirable role of a wave guide carrying part of the GPR e.m. waves along the wall surfaces. Even though the plaster is the primary suspect, we note that the rock itself into which KV62 is carved may have similar e.m. properties. Thus, considering also the reduced dimensions of Tutankhamun's funerary chamber (approximately 6 m x 4 m x 3 m), the waves traveling along the wall surfaces would bounce back to the receiver, carrying with them spurious

information originating from the walls opposite to the one being scanned, and perhaps even from Tutankhamun's massive quartzite sarcophagus, which takes up much of the central burial chamber. This spurious information is what we refer to as *ghost signals.*

It is perhaps of interest to report that in the first two days of our survey, we were misled by these ghost signals but, given the several measuring session and the different acquisition systems, we could cross-check and eliminate the spurious signals. Finally, we agree with the conclusions of the second GPR survey, which did not confirm Watanabe's results (National Geographic Society, 2016). However, probably due to the limited time availability and spatial extension, the second KV62 GPR survey was unable to provide a convincing conclusive answer. Therefore we can conclude, with a high level of confidence, that Reeves' theory concerning the existence of hidden chambers adjacent Tutankhamun's tomb is not supported by the GPR data.

Acknowledgements

We would like to thank Dr. Khaled El-Anany, Egyptian Minister of Antiquities, for believing in the potential of geophysical research applied to archaeology and for promoting the third KV62 radar scan. We are deeply grateful to Dr. G. Capriotti Vittozzi of the Italian Archeological Center in Cairo, for her continuous support, strategic management and valuable discussions on the project. We would also like to thank Dr. Dean Goodman for the GPR-SLICE software support, Dr. Mamdouh El-Damaty, Dr. Nicholas Reeves and Dr. Fred Hiebert for useful and motivating discussions and last but not the least Samir Zaki for his fundamental help in the data acquisition.

This work was supported by the National Geographic Society (NGS Explorer Grant SP 37-16 and Nefertiti Program X10380) and by the Fondazione Novara Sviluppo; Geostudi Astier s.r.l. and 3DGeoimaging also significantly participated to the research expenses.

References

Aubry M. P., Berggren W. A., Dupuis C., Ghaly H., Ward D., King C.,Knox R. W. O'B., Ouda K., Youssef M. and Galal W. F. (2009) Pharaonic necrostratigraphy: a review of geological and archaeological studies in the Theban Necropolis, Luxor, West Bank, Egypt. Terra Nova, 21, 237–256.

Carter H. and Mace A. C. (1923). The Tomb of Tut*Ankh*amen. London: Cassell and Company Ltd.

Daniels, D, J,. (2004) Ground Penetrating Radar, 2nd edition, The Institution of Electrical Engineers, London, pagg. XV- 734.

Dupuis C., Aubry M. P., King C., Knox R. W. O.'B., Berggren W. A., Youssef M., Galal W. F. and Roche M. (2011) Genesis and geometry of tilted blocks in the Theban Hills, near Luxor (Upper Egypt). Journal of African Earth Sciences, 61, 3, 245-267.

El-Aref, Nevine (2015). Discovery of the Century? in Al-Ahram Weekly (Issue 1273, 3-9 November 2015).

Factum Arte, 2015, http://www.highres.factum-arte.org/Tutankhamun/, with additions, copyright © Factum Arte/Ministry of State for Antiquities and Heritage, Egypt.

Fischanger, Federico, et al (2018). *Geophysical anomalies detected by Electrical Resistivity Tomography in the area surrounding Tutankhamun's tomb*, accepted for publication in Journal of Cultural Heritage (18 July 2018).

Goodman D., Nishimura Y. and Rogers J.D. (1995) GPR time slice in archaeological prospection. Archaeological Prospection, vol. 2, n. 2, pp. 85-89.

Goodman D. and Piro S. (2013) GPR Remote Sensing in Archaeology, Springer, pagg. XI-233.

Goodman, D. (2004) GPR-SLICE. Ground Penetrating Radar Imaging Software. User's Manual, Geophysical Archaeometry Laboratory, California, 2004 (http://www.gpr-survey.com/practice/GPR-SLICE).

Hiebert, Fred (2016), Private communication.

Lori Wong (ed.) (2013) The Conservation and Management of the Tomb of Tutankhamen (KV 62): A project bibliography, The Getty Conservation Institute, Los Angeles, California, USA.

Michaelson R., Walker P., 2016, Tutankhamun's secret? Experts hope new chambers could contain tomb of Nefertiti, in The Guardian, 18 March 2016.

Milsom J. and A. Eriksen (2011) Field geophysics. Fourth Edition, Wiley & Sons Ltd, 287 pp. ISBN: 978-0-470-74984-5

National Geographic Society (2016) The kv 62 survey #2 team, Ground Penetrating Radar - kv 62 GPR survey #2: Report to the Egyptian Ministry of Antiquities (unpublished).

Porcelli, F. et al., La Mappatura Geofisica Completa della Valle dei Re: Risultati preliminari del primo anno di attività (2016-2017), in Ricerche Italiane e Scavi in Egitto, Vol. VII (Italian Cultural Institute, Cairo), in press.

Reeves N. 2015, The Burial of Neferiti? (a publication of the Amarna Royal Tomb Project, University of Arizona, Tucson, AZ, USA).

Sandmeier (2018), Reflex 8.55, http://www.sandmeier-geo.de/Download/reflexw_manual_a4.pdf visited on 04/04/2018 h11:00.

Vaccaneo D., Sambuelli L., Marini P., Tascone R. and Orta R. (2004) Measurement System of Complex Permittivity of Ornamental Rocks in L Frequency Band, IEEE Transaction on Geoscience and Remote Sensing, 42, 11, 2490-2498.

Watanabe H. (2015) "Report on the radar survey of the tomb of Tutankhamun (KV 62)", Terra Information, Yokohama, translated by Shohta Ueno and Alexandra J.Park (Copyright @ Hirokatsu Watanabe, 2015, unpublished).

Weeks K. (2003) “The Atlas of The Valley of the Kings”, Theban Mapping Project, American University in Cairo Press, 2003.

Wong L., Rickerby S., Rava A., El- Din A. and Sharkawi M. (2012a) Developing approaches for conserving painted plasters in the royal tombs of the Valley of the Queens, Proceedings of the XI International Conference on the Study and Conservation of Earthen Architecture Heritage, Lima, Peru.

Wong L., Rickerby S., Phenix a., Rava A. and Kamel R. (2012b) Examination of the wall paintings in Tutankhamen's Tomb: Inconsistencies in original technology, Contribution to Vienna Congress, The J. P. Getty Trust. DOI 10.1179/ 2047058412Y.0000000035.

Wust R. A. J. and J. McLane (2000) Rock deterioration in the royal tomb of Sethi I, Valley of the Kings, Luxor, Egypt, Engineering Geology, 58, 163-190.

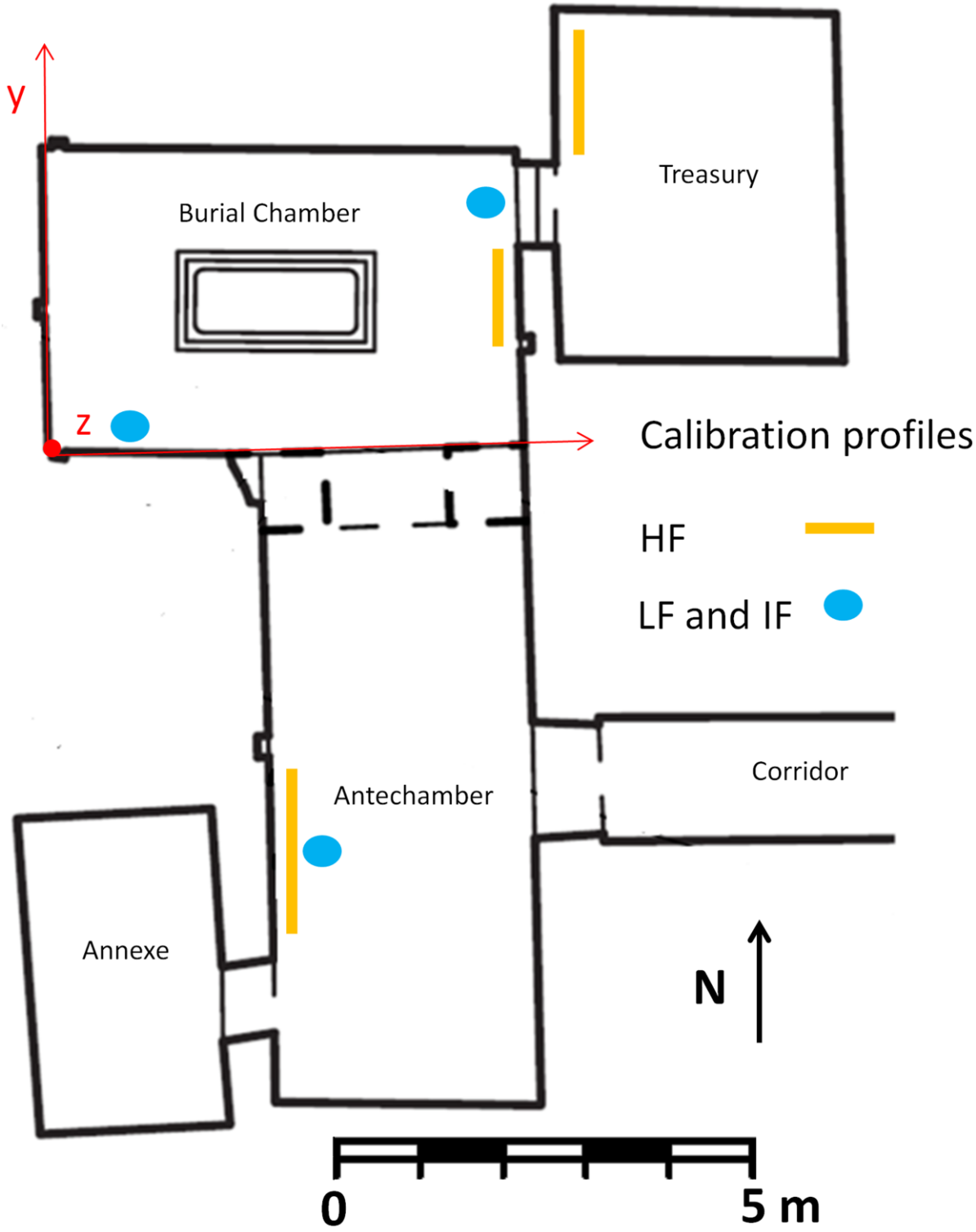

Figure 1: *plan view of the KV62 with indication of the reference system used for survey positioning and the location of the calibration profiles: yellow lines are the HF scans profiles, cyan dots are the planar projection of the vertical LF and IF profiles (modified from Weeks, 2003).*

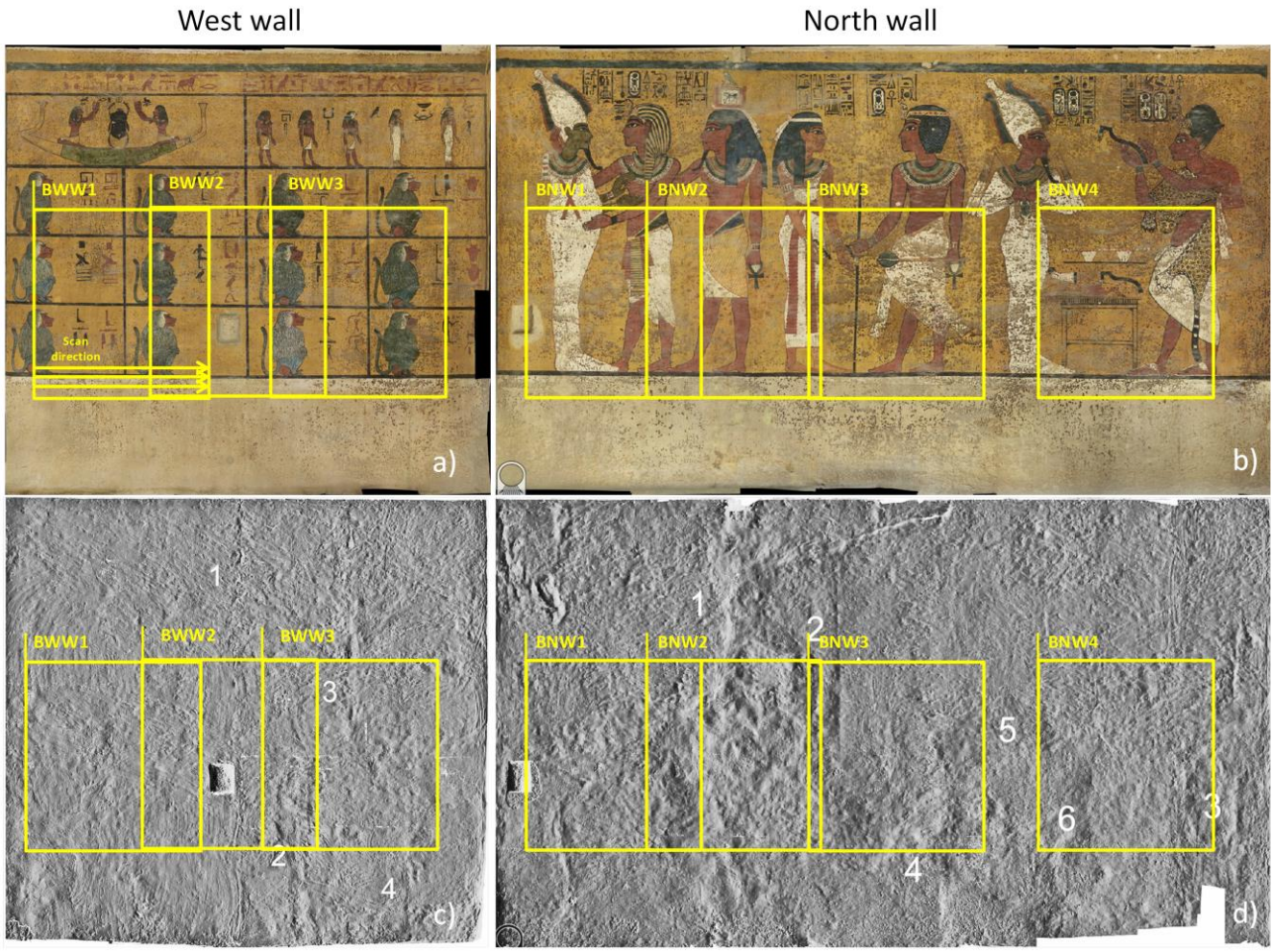

Figure 2: *The positions and the areas covered by the HF surveys along the West and North walls (yellow polygons) superimposed to pictures of the walls (in a and b) and to laser scans images (c and d); In a the scan direction and approximate spacing (constant for every panel) is also indicated; Numbers in c and d refers to Reeves hypotheses and respectively: in c) 1 and 3 natural faults in the rock, 2 and 4 artificially defined edges, in d) 1 natural, 2 and 3 artificially cut, 4-6 outline of an internal doorway (modified from Reeves, 2015).*

Figure 3: *Pictures taken during LF and IF radar scans showing: a) and b) the IDS TR200 shielded antenna and c) the multi-channel IDS Stream-C system deployed by the lifter.*

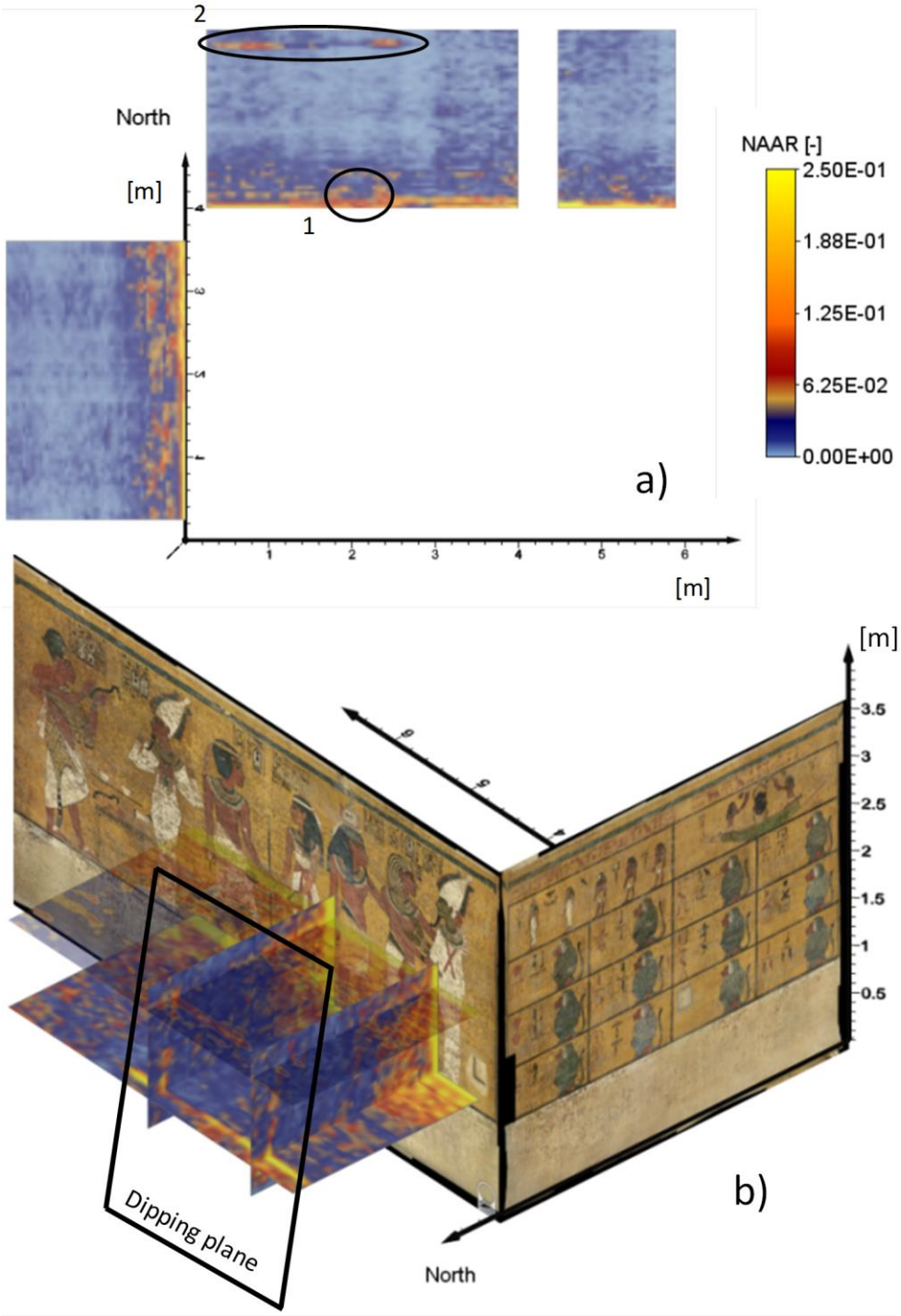

Figure 4: *HF-TM mode processed data: a) Top view of the sections at 1 m from the floor, with evidence of: 1) high amplitude shallow events related to the wall repair and 2) a 2 m deep linear reflection event; b) 3D view of some significant sections: behind the North wall, a clear fracture plane emerges from the combination of vertical and horizontal sections.*

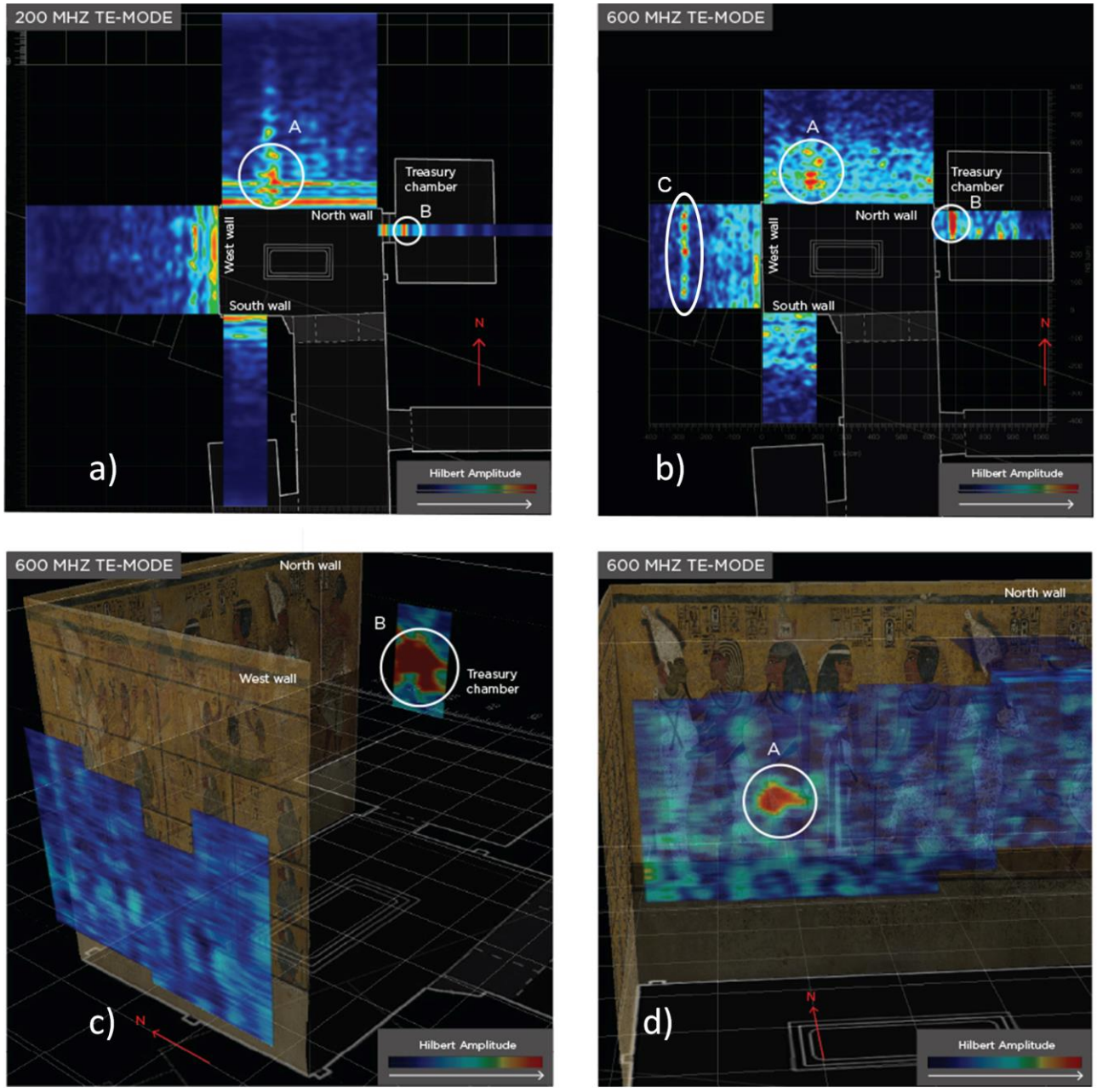

Figure 5: *IF and LF processed data: top view of representative horizontal cross sections for a) LF processed data and b) IF processed data, vertical cuts at 0.6 m depth from the IF GPR volume (TE-mode) behind the west c) and north wall d) are also reported. Evidence of: A wall repair anomaly, B wall separating the Burial Chamber from the Treasury Chamber and C deep linear reflection event are reported in all the panels.*

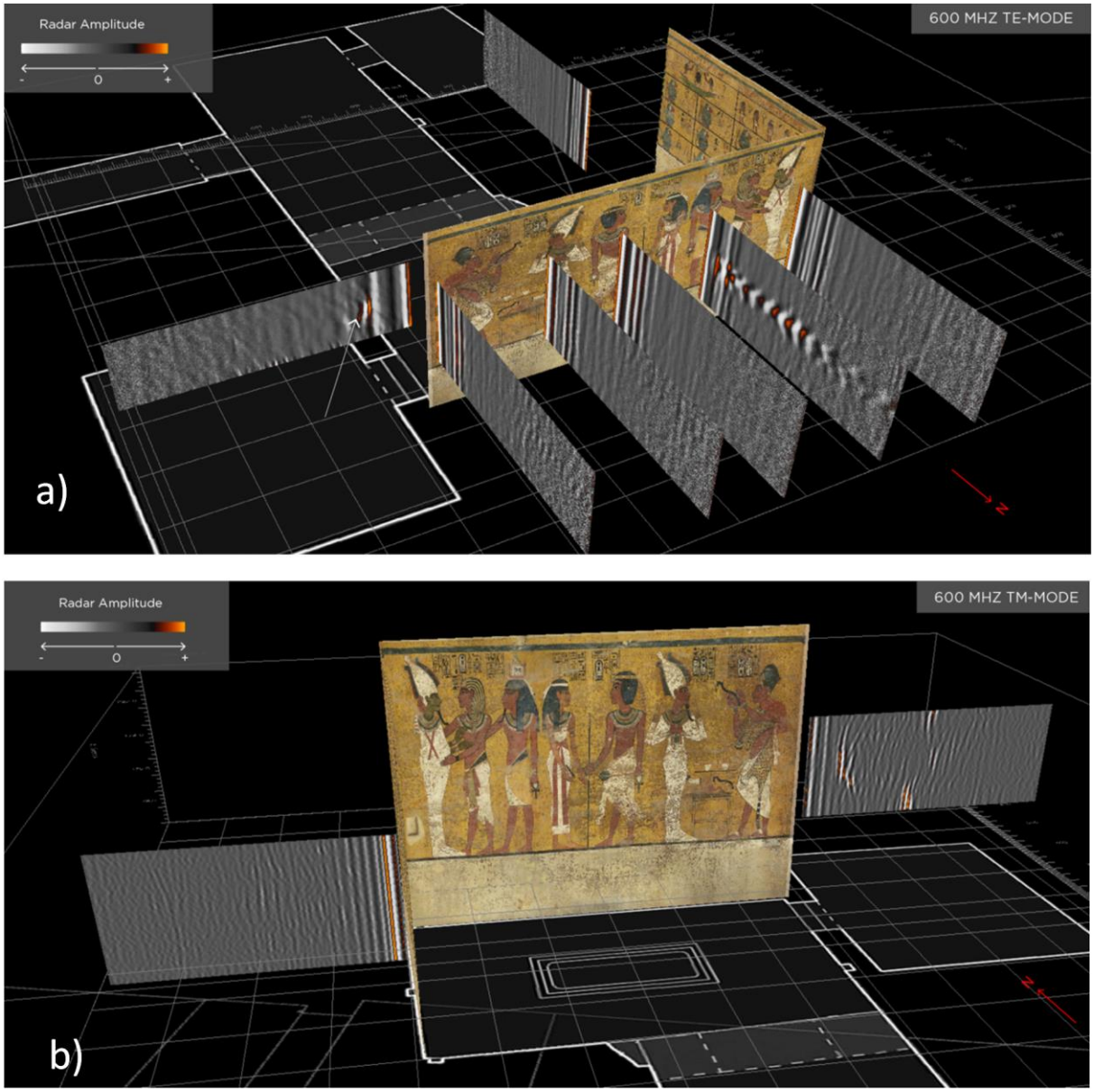

Figure 6: *IF processed data: perspective view of IF scans showing the response recorded from: a) the North, East and South walls and b) from the East and West walls.*

SUPPLEMENTARY MATERIAL

TO

The third KV62 radar scan: Searching for hidden chambers adjacent to Tutankhamun's tomb.

1. Data acquisition

The wooden frame was designed for HF scans is reported in Figure 1S. This frame was used starting from the third day of the surveys in an attempt to attenuate the significant diffractions from the vertical lateral supports observed in the radargrams during the first two days, which were performed with a similar aluminum frame. Given the presence the sarcophagus lid resting on the floor of the burial chamber, we also built a wooden platform to pass over it (Figure 1S). In order to compensate for the highly irregular floor surface, we leveled a wooden slab that we used as base for the frame.

The GPR profiles distribution for the LF dataset is shown in Figure 2S, where the white arrows represent the position of the radargrams collected along the KV62 walls. Note that in the NE corner of the North wall, the same wooden platform used for HF scans was adopted in order to pass over the sarcophagus lid, so that the starting acquisition height in this location was higher than for the other profiles.

The GPR profiles distribution for the IF dataset is shown in Figure 3S, where white arrows and the cyan arrows represent the respective distribution of the radargrams acquired in TM (336 radar profiles) and TE (126 radar profiles).

2. Data processing

The three collaborating groups rocessed the data acquired with the different GPR systems independently and with different software, to avoid biasing and cross influences. Only after a satisfying processing step was reached we discussed and uniformed the processing flows in order to obtain a consistent result for all the surveys. Final processing steps adopted for the different GPR systems are hereafter reported.

2.1 High Frequency (HF) scans.

After many trials, a processing sequence that we consider appropriate in order to extract useful information without meaningful alteration of the raw data has been achieved for the HF scans. Data processing has been performed with Reflexw 8.55 (Sandmeier, 2018). The adopted processing steps were:

1. subtract-mean(dewow), to attenuate very low frequency components likely due to the acquisition setup;
2. move start time (-2.4 ns), to correct for the air gap between the antenna and the wall surface and to system delay;
3. divergence compensation, to recover the geometrical spreading of the wave front; since the e.m. properties of the plaster and of the hosting rock are not known with sufficient accuracy, we did not apply any other gain based on the physical attenuation;
4. bandpass 4-poles Butterworth filter (1400 – 3400 MHz), to attenuate low and high frequency noise in the traces; cut-off frequencies have been selected after spectral analysis carried out on randomly selected sample radargrams;
5. background removal, to remove strongly constant horizontal banding that, in this context, we attribute to a ringing of the pulse due to the air gap between the antenna and the wall and due to the widespread presence of the plaster;
6. spectral whitening, to widen the frequency band and shorten the pulse duration enhancing localized reflection events; this step is associated to a further bandpass four-poles frequency filter (900-1200, 3700-4000 MHz) to further attenuate low and high frequency noise in the traces due to whitening;
7. time cut (36 ns), to focus the investigation onto a depth were we judge there is relevant information.
8. f-k velocity band-reject filter from 0.135 to 0.3 m/ns to further reduce any residual effects of the diffractions from the vertical lateral supports, still partially evident even after the wooden frame was adopted (see Sec. 2.1 above).

Examples of the results obtained by the adopted processing steps will be given in the following over calibration profiles. Finally, processed radargrams were assembled in space using the surveys reference system (see Figure 1 of the paper), while the software Voxler® 4.3.771 (Golden Software, Colorado, USA) was used to obtain a 3D imaging of the surveys. For this purpose, the absolute reflection amplitude was computed for each sample of the traces and the traces were interpolated with an inverse distance power-2 isotropic algorithm with a spatial resolution of 0.04 m in the x,y and z directions.

2.2 Low Frequency (LF) and Intermediate Frequency (IF) scans.

Raw data from LF and IF scans were post-processed and imaged with GPR-Slice software (Goodman et al, 1995; Goodman et al., 2004). The adopted processing steps were similar for the two surveys up to a certain level where dedicated processing was carried out. The processing steps for LF scans included:

1. move start time , to correct for the air gap between the antenna and the wall surface and for the system delay;
2. apply a gain function, to enhance the reflectors of interest without introducing clipping effects and artifacts into the data; a user defined gain function containing a linear component and an exponential compensation factor was applied. The total gain factor was selected according to the energy level exhibited by the radar pulse energy.
3. wobble noise correction; to attenuate the low frequency noise a wobble filter was used to compute a running average over a fixed scan length and then subtract it from the radar scans.
4. frequency-wavenumber (FK) filtering; after a spectral analysis was performed in the frequency-wavenumber domain, a FK filter was used to suppress the data noise observed by removing specific spatial frequency components.
5. bandpass filtering (128 - 365 MHz), to attenuate the horizontal band caused by the air gap between the antenna and the wall and to suppress high frequency noise.

6. Cepstrum deconvolution, to smooth out amplitude undulations in spectral frequencies, and to reduce the influence of multiple reflections.
7. Box-car filtering, to attenuate incoherent noise arising from the cepstrum deconvolution.

The same first three processing steps of LF scans have been used for IF scans also, followed by a bandpass filtering. Calibrated parameters have been adopted to account for the different radar system employed (i.e. for the IF scans the adopted parameters were: move start time of -12.8 ns and cutting frequencies of 330 and 890 MHz). A further spectral whitening step was also adopted, to equally weigh all the spectral components with the same magnitude and to increase the gain in portions of the radargrams with lower amplitude. The final processing step of IF data was a FK filtering similar to the one used for LF scans to attenuate the high frequency noise induced by the spectral equalization process.

Examples of the results obtainable with the adopted processing steps will be given in the following over calibration profiles. We finally Hilbert-transformed both LF and IF processed radargrams, in order to eliminate phase components before assembling the dataset and compiling 3D vector volumes. We also computed gain calibration curves for the multi-channel dataset to compensate variations in channels gain levels. Finally, we compiled GPR volumes using cell size of 0.05 m, where profiles spacing in the IF and LF ranges from 0.0435 to 0.2 m, and computed on a sequence of 269 and 225 height levels for the two respective datasets, corresponding to steps of about 0.01 m. We then interpolated the volumes along the cross-line direction only where gaps between adjacent lines exist. For this purpose, we compiled and interpolated two independent volumes for two walls oriented along the N-S and the E-W. We finally merged interpolated volumes into a unique 3D volume and smoothed with a 3x3x3 low pass filter.

3. Results over Calibration Profiles

Successful imaging of known voids and structures over calibration profiles was used to test the processing sequence and to evaluate the potentiality and limitations of the adopted surveying approach. In Figure 4S, examples of processed HF calibration profiles acquired along the East Wall of the Burial Chamber

to the Treasury room (for the exact locations, see Figure 1 in the paper) are reported. For these locations, the wall surface is cover by a plaster layer and by paintings similarly to the West and North walls of KV62 funerary chamber.

A clear difference can be observed in the two acquisition modes. The TE mode is successful in evidencing the presence of the void related to the Treasury room, with a clear reflection event located at a depth of 0.55 m, that matches the actual wall thickness in this particular location. Conversely, no clear reflections appear on the TM mode. The differences between the two acquisition modes go beyond those that are normally expected from the different polarizations over a reflecting plane parallel (even if gently "waving") to the antenna profile. Similar differences and similar results have been also observed in the calibration profiles acquired from the Antechamber to the Annex (see Figure 1 in the paper), where only the TE mode was successful in locating the known void at a correct depth of 0.8 m. In this location the wall surface is free from the plaster.

Differences between the two acquisition modes are also observed in the HF calibration profiles acquired from the Treasury room to the Burial Chamber (also a plaster-free surface, for its exact location see Figure 1 in the paper) reported in Figure 5S. A clear diffraction hyperbola is evidenced particularly for the TE mode. The hyperbola position, both in time and space, and the fact that it is much clearer in TE mode, led us to conclude that it is likely due to the corner of the door between the Burial chamber and the Treasury room. This has also been confirmed by forward modeling simulations of the radar wave propagation over an on-purpose built model of the Burial chamber. The aforesaid hyperbola gave also a clear estimation of the propagation velocity (0.12 m/ns) of the GPR pulse in the rock around the tomb.

We also performed calibrations profiles for LF and IF acquisition modes. The calibration profiles performed over known wall thickness ranging from 0.55 m (wall separating the Burial Chamber from the Treasury Room) to 0.8 m (wall between the Antechamber and the Annex) were successful in detecting the backwall and determining the correct thickness of the walls. In Figure 6S, examples of the calibration profiles for LF scans are reported, with similar results obtained also for the IF scans.

Conversely, both IF and LF calibration profiles performed along the south wall of the Burial Chamber (for exact location see Figure 1) failed in locating the known void of the Annex at about 5 m depth. This gave us indications that attenuation factors are higher than expected and shorter maximum investigation depths, particularly for LF scans, should be expected.

In all the frequency bands used for our GPR scans, we found clear differences in the TE and TM modes of operation. In HF scans vertical corners (e.g. the corner of the door between the Burial chamber and the Treasury room in Figure 5S) are clearly, and correctly, detected in the TE mode acquisition and nearly absent in TM mode. On the other hand, we do not have a clear explanation for the very low reflection intensity of TM mode within the calibration profiles, where the reflectors are planes (even if gently “waving”) parallel to the antenna profiles (the East wall of the Annex or the West wall of the Treasury). These differences go beyond those that that are normally expected from the different polarizations.

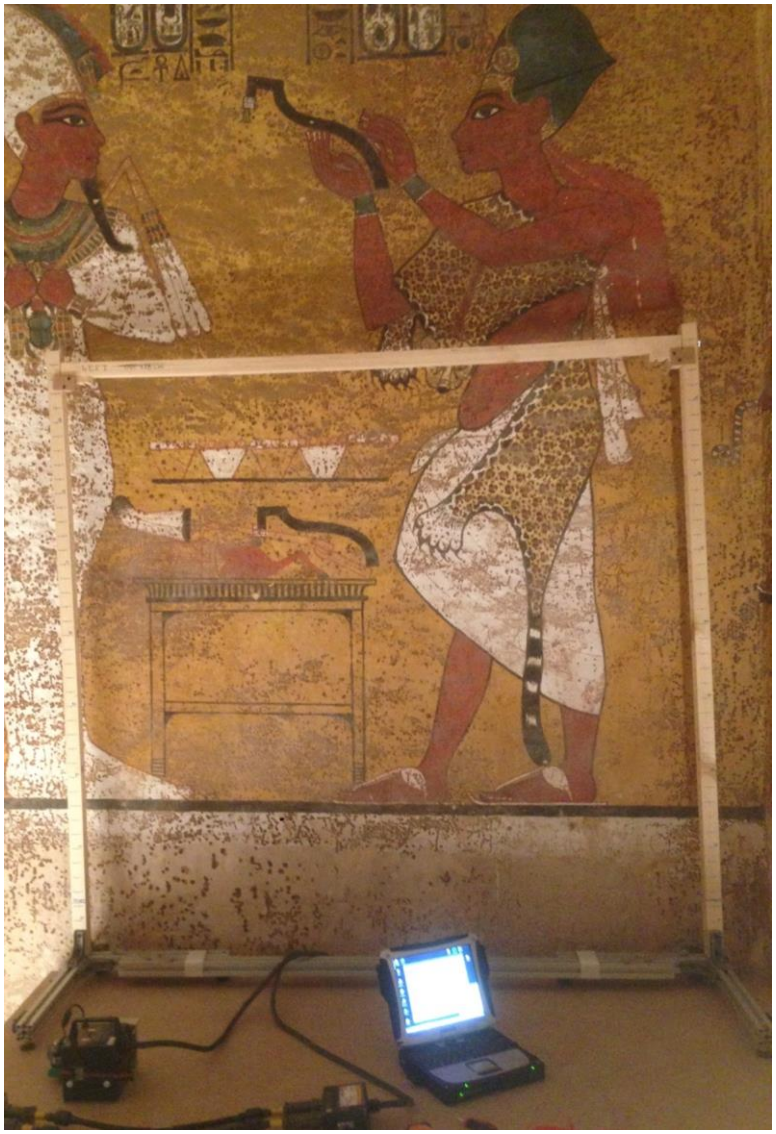

Figure 1S: *Picture taken during HF radar scans showing the wood frame over the wooden platform in the right side of the North wall where the sealed doorways is supposed.*

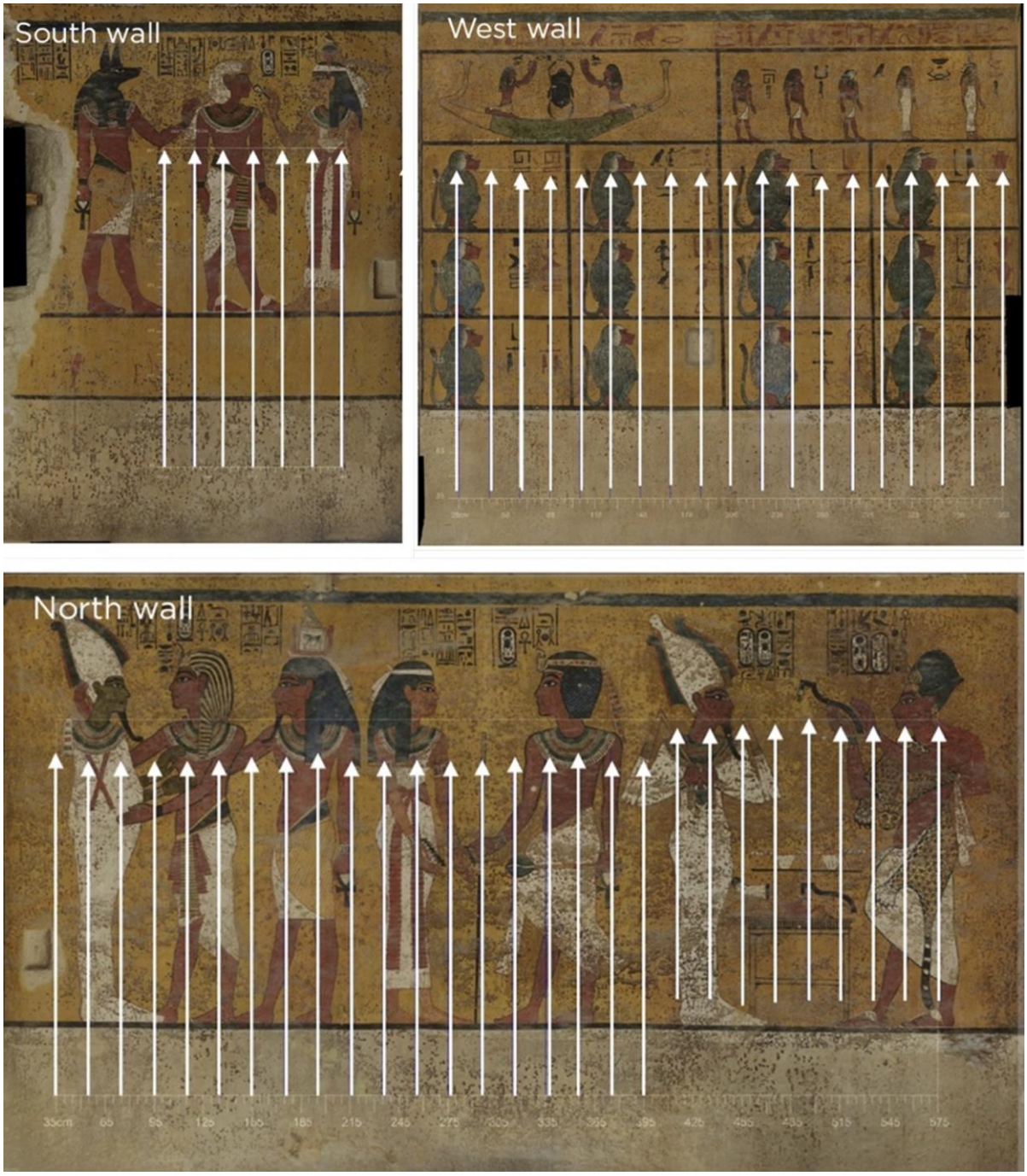

Figure 2S: *LF radar profiles acquired with the IDS TR200 GPR unit along the KV62 walls, the spacing among the lines is of 0.2 m.*

Figure 3S: *IF radar profiles acquired with the multi-channel IDS Stream-C system along the KV62 walls, white arrows represent the position of the radargrams acquired in TM-mode, at fixed spacing of 0.0435 m; cyan arrows represent radargrams acquired in TE-mode at fixed spacing of 0.099 m.*

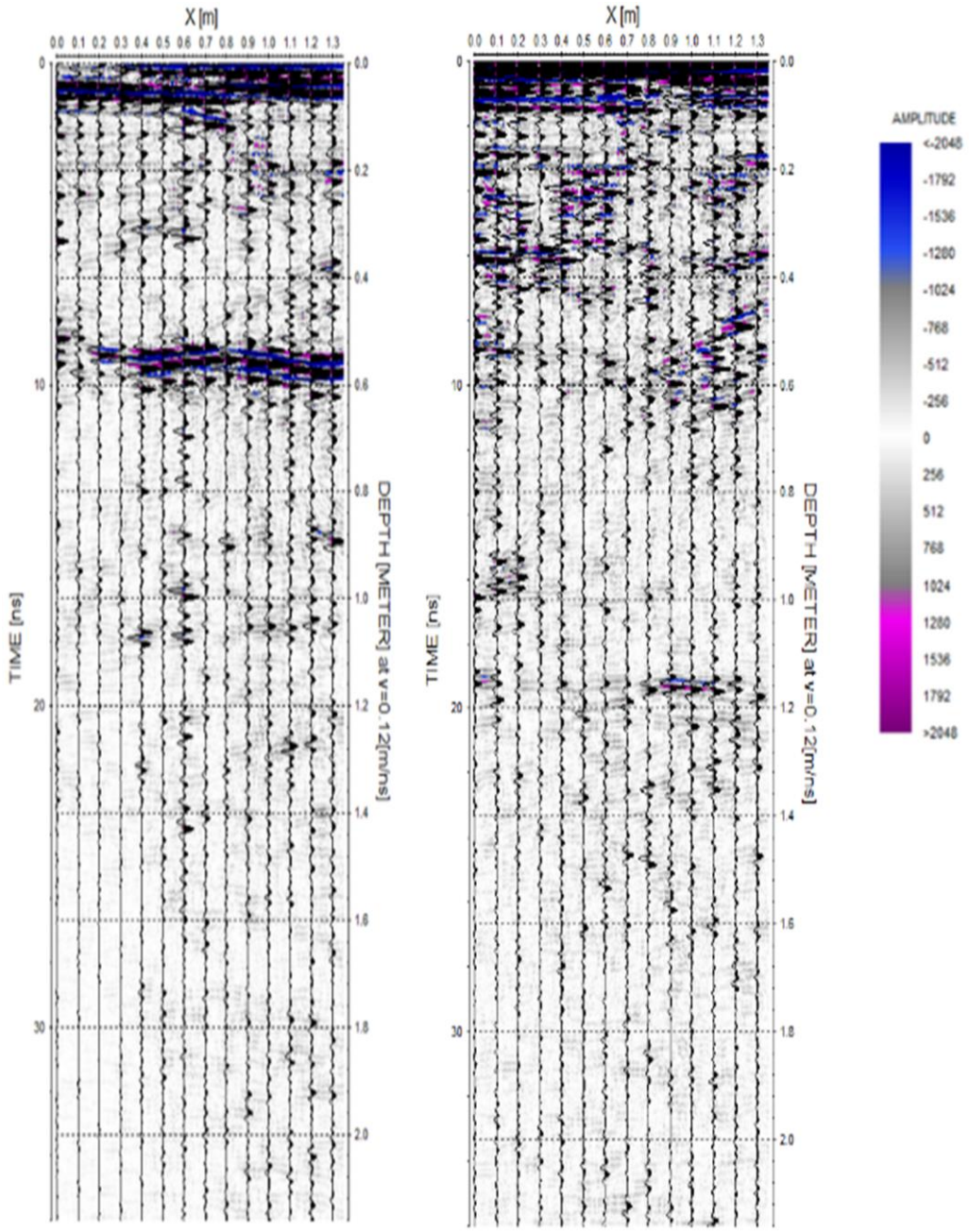

Figure 4S: *Processed HF calibration radargrams acquired from the Burial Chamber to the Treasury room (for exact location see Figure 1 in the paper): left) TE mode and right) TM mode.*

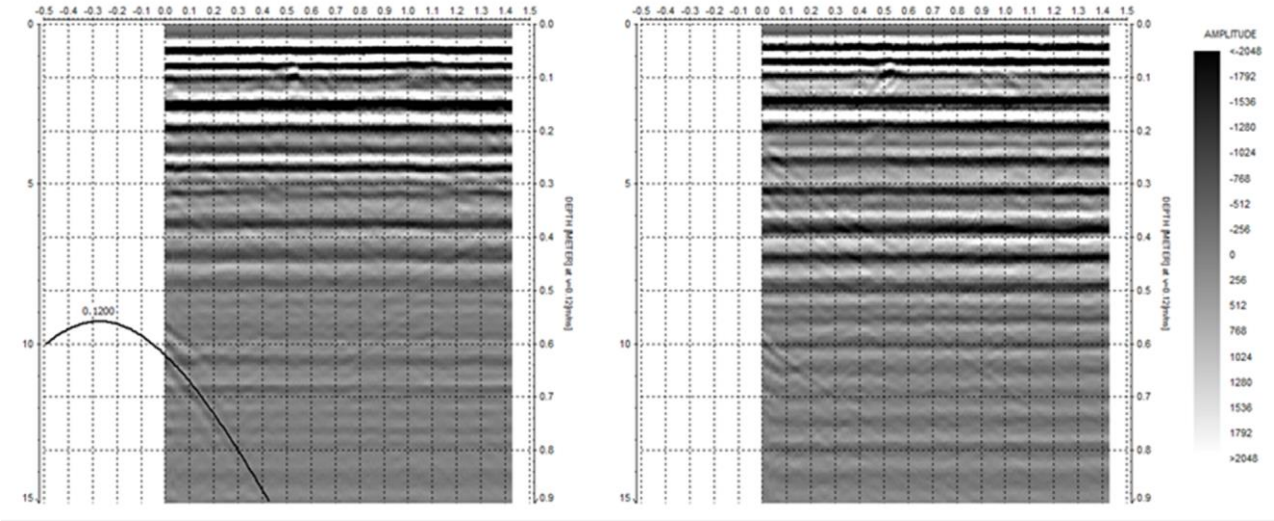

Figure 5S: *HF calibration radargrams, at processing step 02, acquired from the Treasury room to the Burial Chamber (for exact location see Figure 1 in the paper): left) TE mode and right) TM mode.*

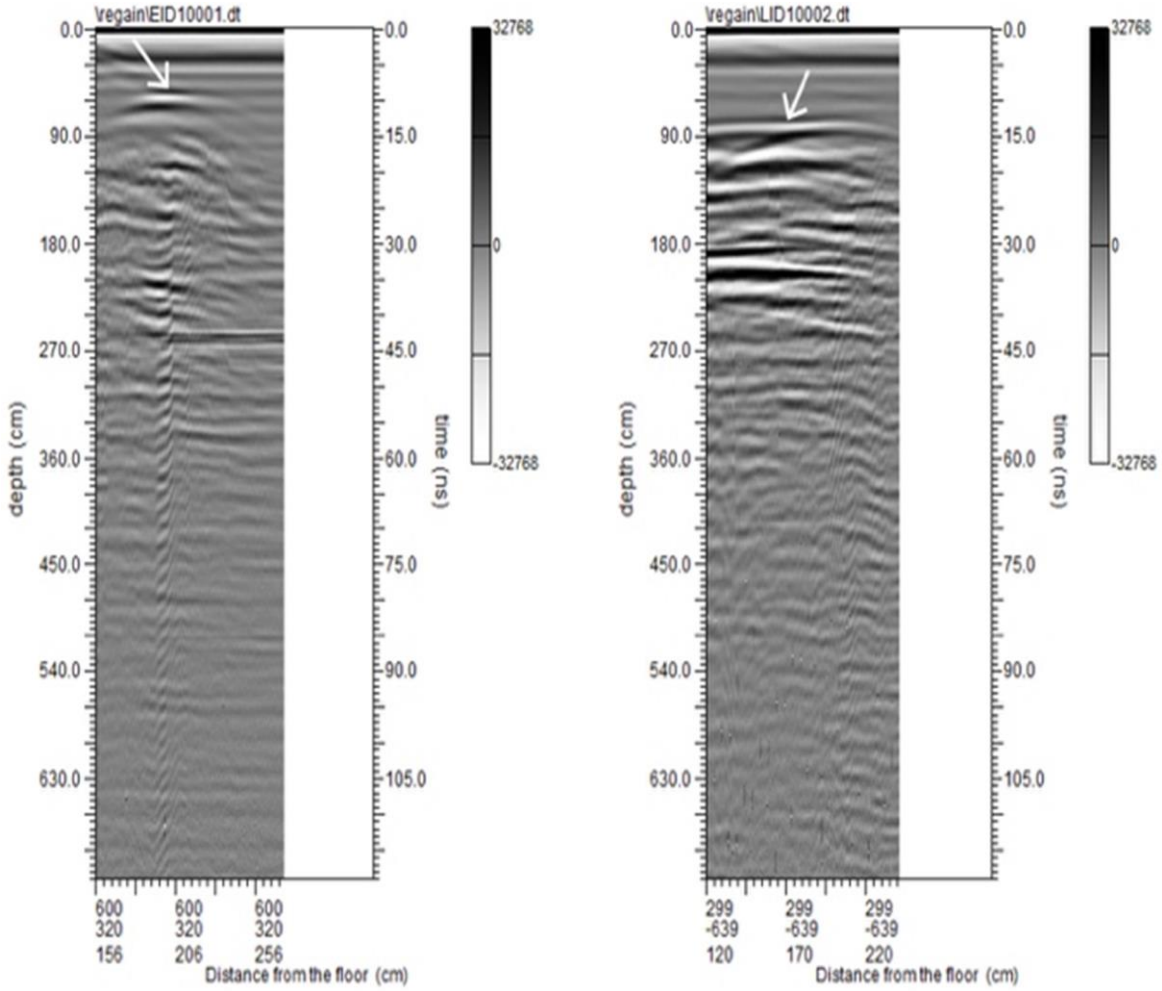

Figure 6S: *LF calibration radargrams, at processing step 03, acquired along the East Wall of the Burial Chamber toward the Treasury(left) and along the West Wall of the Antechamber toward the Annexe (right),for exact location see Figure 1 in the paper.*